Direct measurement of spontaneous charge migration across anatase–brookite nano–heterojunctions

Leonardo Lo Presti[1,2], Valentina Pifferi[1], Giovanni Di Liberto[1,3], Giuseppe Cappelletti[1], Luigi Falciola[1], Giuseppina Cerrato[4], and Michele Ceotto[1,*]

[1.] Department of Chemistry, Università degli Studi di Milano, via Golgi 19, 20133 Milano

[2.] Istituto Nazionale di Fisica Nucleare (INFN), Laboratori Nazionali di Frascati, Via Enrico Fermi 40, 00044 Frascati

[3.] Present address: Department of Materials Science, Università degli Studi di Milano–Bicocca, via Cozzi 55, 20125 Milano

[4.] Department of Chemistry, Università degli Studi di Torino, via Giuria 7, 10125 Torino

* To whom correspondence should be addressed: michele.ceotto@unimi.it

SUPPORTING INFORMATION

Index

S1. Experimental setup

Commercial titanium dioxide powders are purchased by Alfa Aesar (Anatase 9.5, 42, 130 and 284), Sigma–Aldrich (Brookite) and Sachtleben (Hombikat UV 100). Home–made powders are prepared by varying anatase/brookite quantity, following a previously optimized sol–gel synthesis[1] based on the addition of triethylamine (TEA). They are labelled TN_0.05, 0.1, 0.2, 0.4 and 0.5, indicating the nominal N/Ti molar ratio used during the synthetic procedure, apart for T400, which is synthesized without the addition of TEA. A deep physico–chemical characterization is performed for all the tested samples from the structural, morphological and optical point of view.

Room-temperature X-ray powder diffraction (XRPD) patterns were collected between 20° and 80° (counting time of 20 s for each a 0.1 step) with a Philips PW 3710 Bragg−Brentano goniometer equipped with a scintillation counter and 1° divergence slit, 0.2 mm receiving slit, and 0.04° Söller slit systems. We employed graphite-monochromated Cu Kα radiation at 40 kV × 40 mA nominal X-rays power. Rietveld refinement has been performed using the GSAS software suite and its graphical interphase EXPGUI.[2] Volume–averaged crystallite dimensions have been estimated through Scherrer equation on (101) anatase and (211) brookite reflections.

HR-TEM images were obtained by means of a JEOL 3010–UHR Instrument equipped with a LaB_6 filament (acceleration potential 300 kV). All digital micrographs were acquired by an Ultrascan 1000 camera, and the images were processed by Gatan Digital Micrograph program version 3.11.1. Samples were dry dispersed onto Cu grids coated with “lacey” carbon film before the analysis.

The specific surface areas were determined by the classical BET procedure using a Coulter SA 3100 apparatus. Desorption isotherms were used to determine the pore size distribution using the Barret–Joyner–Halander (BJH) method with cylindrical pore size.

Diffuse reflectance spectra of the powders were registered with a UV–vis scanning spectrophotometer (Perkin-Elmer, Lambda 35), which was equipped with a diffuse reflectance accessory. A “total white” Perkin-Elmer reference material was used as the reference. All spectra were acquired by working in reflectance mode and Kubelka–Munk elaboration is applied for the band gap evaluation.

The cell for electrochemical measurements was equipped with a saturated calomel and two platinum wires as reference and counter electrodes, respectively. The working electrode is a Fluorine doped tin oxide glass (FTO, Sigma Aldrich, 2.3 mm thick ≈ 7 Ω sq^{-1} surface resistivity) covered with a deposition of the desired sample placed close to a Lugging’s capillary. The immobilization of TiO_2 powders is carried out by dispersion in 2–propanol (2 mg/mL), sonication for 5 minutes and deposition by a Spin150 spin–coater (SPS, ATP GmbH, 2000 rpm, 20 s, 8 layers) on FTO, previously washed in 2–propanol (Sigma–Aldrich). The as-prepared films are finally sintered at 400°C in air for 1 h to improve film adhesion and homogeneity. The supporting electrolyte is deaerated (with nitrogen) $NaClO_4$ 0.1 M. Analyses are carried out by using a potentiostat/galvanostat PGStat30 (Autolab, The Netherlands) equipped with a FRA (Frequency Response Analyzer) module and Nova 2.0 software. Electrochemical Impedance Spectroscopy (EIS) is performed at 0 V (SCE) (amplitude 0.01 V, range of frequency 0.01–10000 Hz) and Zview software is employed for the fitting.

Photocurrent measurements are registered in the previous electrochemical cell at a fixed potential of +1 V (SCE) (step potential 0.1 s) under 500, W UV light irradiation (Jelosil HG 500, iron halides).

The first 600 s represent the dark current, then 200 s of irradiation are alternated with 100 s at dark for 6 times.
Photocatalysis experiments have been performed using a 300W solar lamp emitting in the 380–600 nm range of wavelengths, with nominal intensity $I = 1.2\times10^{-5}$ Einstein dm^{-3} s^{-1}. Reagent–grade methylene blue, NO_x and toluene have been considered as substrates.

NO_x photodegradations were carried out in a pyrex glass cylindrical reactor (with an effective volume of 50 dm^3) and irradiated with the solar lamp described above at room temperature. The relative humidity was kept constant in all the runs (50%). Air, NO_x and N_2 gas streams were mixed to obtain the desired concentration (500 ppb), introduced inside the photoreactor and the photodegradation products concentrations (NO and NO_2) were continuously monitored by an on-line chemiluminescent analyzer (Teledyne Instruments M200E).

Photoremoval of toluene were conducted in a Pyrex glass cylindrical reactor with diameter of 200 mm and effective volume of 5 dm^3, loaded with 0.5 g of catalyst in the form of powder deposited from 2-propanol slurry on flat glass disk. The gaseous mixture in the reactor was obtained by mixing hot chromatographic air, humidified at 37%, and a fixed amount of volatilized (250 °C) toluene. The initial concentration of toluene in the reactor was 1000 ppm; micro-GC sampling allowed us to determine the actual concentration of the contaminant. Toluene and its intermediate oxidation products were analyzed on the eluate solution obtained by washing the catalyst with Milli-Q water, by means of HPLC (Agilent, Model HP 1100; column: ACE 5 C 18, 150 × 4 mm, 60/40 methanol/H_2O, toluene peak at 10.3 min).

As for the last contaminant (methylene blue), the TiO_2 powder was stained with 500 μL of the indicator and allowed to dry. Specimens were subsequently irradiated in air by the solar lamp for 7 h at room temperature. The disappearance of the contaminant in dry condition was followed by analyzing the powders through diffuse reflectance spectra acquired in the vis-NIR range from 350 to 1200 nm using a JASCO/UV/vis/NIR spectrophotometer model V-570 equipped with a barium sulphate integrating sphere. A block of mylar was used as reference sample following a previously reported procedure.[3]

S2. HR-TEM analyses

S2.1 Detailed experimental setup

In order to investigate the ultimate morphology of the anatase-brookite TiO_2 sample, HR-TEM investigations have been carried out on several aliquots of the synthesized material. Images reported in Figure 1 (main text) and Figure S1 below are statistically representative of the whole powder.
The sample consists of closed packed particles in which a very high crystalline nature is evident, as almost all particles exhibit fringe patterns. As for their dimensions, these entirely fall in the nanometric range, being their average size included in the 4-6 nm range.
If we inspect in some detail the fringes patterns evident for these different TiO_2 nanoparticles, two families of crystalline planes are present. The presence of the anatase TiO_2 can be revealed for the nanoparticles with blue contour, and through the (101) family of planes with d = 0.35(4) nm [anatase ICDD card nr. 21-1272]. The presence of the brookite polymorph is proved by analysis of the fringes pattern due to the nanoparticles with white contour, for which the d = 0.35(0) nm distances are highly compatible with the (201) family of planes [brookite ICDD card nr. 01-075-1582]. Both assignments are further confirmed by the analyses of the electron diffraction patterns obtained for both nanoparticles. See Figure 1 in the main text and Figure S1 SI for some examples.

Supplementary Figure 1.

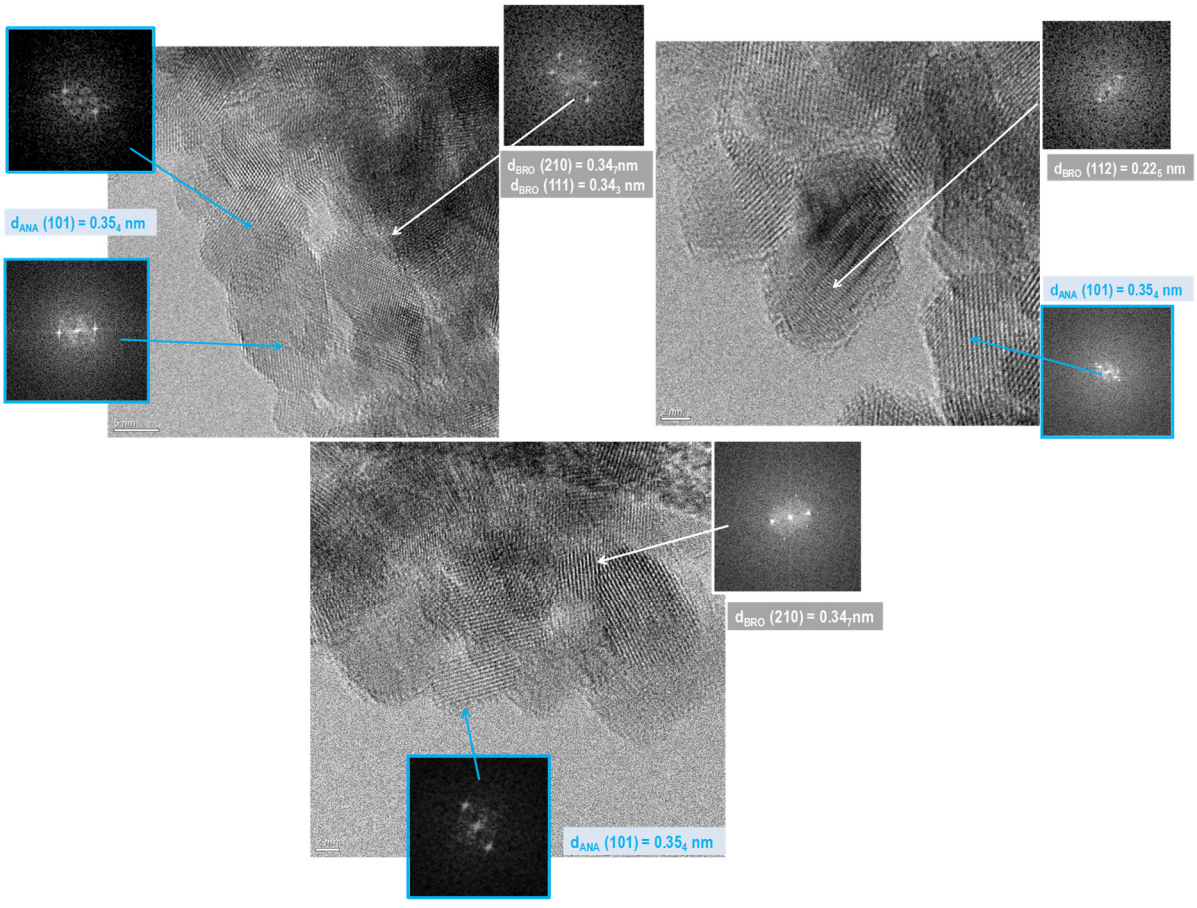

S3. DFT calculations

S3.1 Computational set–up

Simulations are performed employing a plane wave approach by means of the VASP package. The projector augmented pseudopotentials are employed, including spin–polarization.[4] The exchange and correlation functional is described by the Generalized Gradient Approximation (GGA)[5] with the Perdew–Burke–Ernzerhof (PBE) parametrization.[6] To account for electron–screening, the DFT+U [7] has been considered and set for Ti 3d states at the value U=3.0 eV, in agreement with previous works on TiO_2.[8–12] First, independent anatase and brookite phases have been simulated. A 3X3X3 supercell was generated from the primitive one of anatase, resulting into 162 atoms, while in the case of Brookite a 2X2X1 supercell was modeled containing 96 atoms. Calculations have been performed by sampling a 2X2X2 k–point grid. The optimized lattice constants are within 1% deviation from the experimental values. Then, the individual optimized structures have been elaborated to build an anatase:brookite interphase model as detailed in Section S2.3 below. Unless otherwise stated, computational parameters have been kept equal to those employed to model the individual phases.

S3.2 The standard approach: Tersoff band alignment

To gain insights into the interaction between electronic structures of different semiconductors in close contacts, it is mandatory to align their electron bands on the same energy scale. A way to do it has been proposed by Tersoff[13,14] and consists in the evaluation of the so–called Branch Point Energy (BPE, eq. (3))[13] by averaging the Kohn–Sham orbital energies over the k–points:

$$E_{BPE} = \frac{1}{2N_k}\sum_{k=1}^{N_k}\left[\frac{1}{N_{vb}}\sum_{i=1}^{N_{vb}}\varepsilon_i^{vb} + \frac{1}{N_{cb}}\sum_{i=1}^{N_{cb}}\varepsilon_i^{cb}\right] \qquad \text{Eq.(1)}$$

Here ε_i^{vb} and ε_i^{cb} are the state energies in valence and conduction bands, and N_{vb} , N_{cb} and N_k are the number of valence band states, conduction band states, and k–points, respectively. When an interphase is present, the discontinuity in Born–Von Karmán periodic boundary conditions allows non–oscillatory wavefunctions that decay exponentially from one phase into the other. These are associated to Virtual Gap States (ViGS) with imaginary **k**'s, whose energy eigenvalues fall within the gap. BPE is the point where the character of these states switches from being predominantly valence–like (or donor–like) to conduction–like (or acceptor–like), that is, corresponds to an electroneutral state with null tendency to donate or accept charge. If a generic interphase between materials A and B is considered, a Fermi level of A below BPE is predominantly donor–like: possible electron transfer from A to B is favored when the Fermi level of B lies above BPE, and *vice–versa*. As for the present case, approximation is necessary for many atom systems and a number of states around $N_{vb} = N_{cb} = N_k = 2$ has been employed.[15,16] Results for both stoichiometric and defective anatase, aligned with bulk brookite, are shown in Figures S2 and S3.

Supplementary Figure 2.
Density of States (DOS) of Anatase (black line) and Brookite (red line). In Panel (a) the band alignment is done by fixing at zero the Fermi energy of the two (independent) systems. In Panel (b) the zero is set at their respective BPE values. Results are very similar, and they do not suggest any preference of photoexcitation. Band gap underestimation is typical of the plane wave approach.

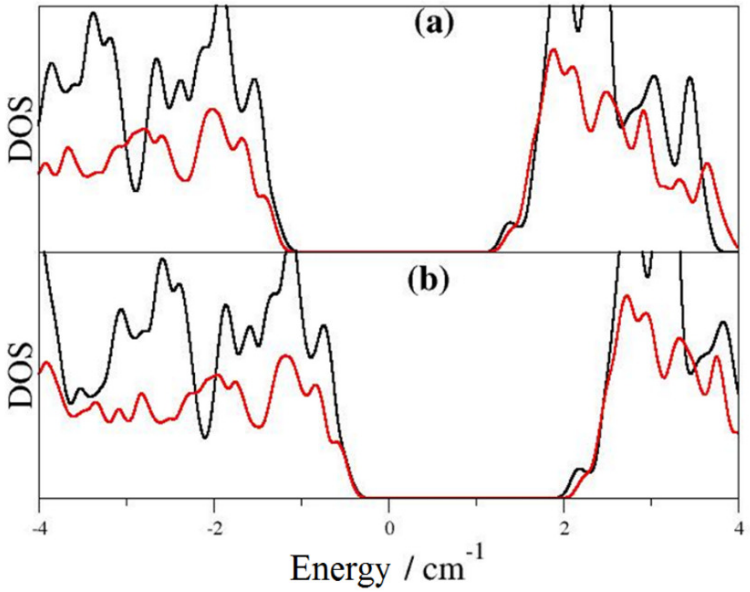

Supplementary Figure 3.
Density of States of defective Anatase (Black line) and Brookite (Red line). In Panel (a) the zero of energy is the Fermi energy of the two systems, while in Panel (b) the zero is set at their BPE. The presence of an oxygen vacancy is indicated by the two shallow mid–gap states below the conduction band. As in Figure S2, no clear conclusions about electronic excitation preference can be drawn.

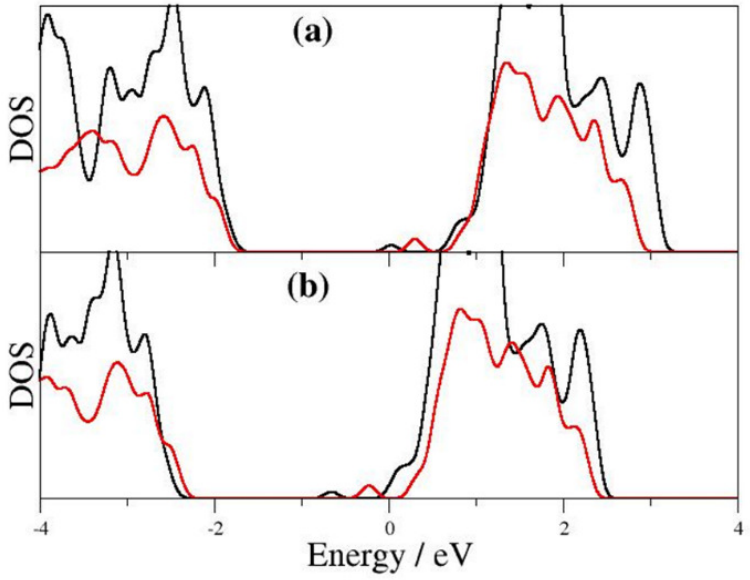

Supplementary Figure 4.
Comparison between anatase and brookite DOS calculations using the plane wave approach (VASP) reported in panel (a) and the atom–centered approach (CRYSTAL) DOS reported in panel (b).[17,18] For the CRYSTAL calculation the PBE0 functional has been employed.[19] Band alignment has been performed using the BPE. Band gap values are quite different, and no conclusions can be reached about possible interphase electronic transfer preferences.

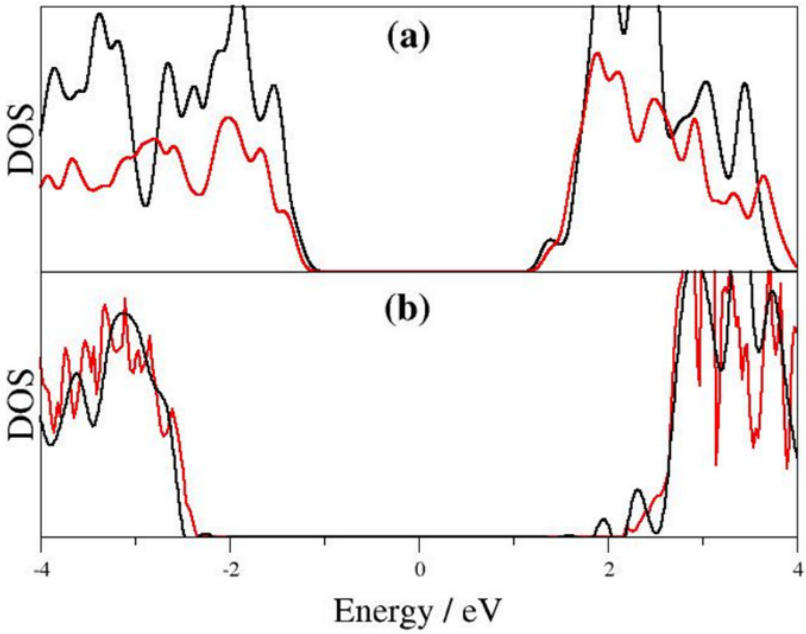

S3.3 The novel approach to build the Anatase/Brookite interphase

Anatase and brookite slabs have been designed separately from the previously optimized bulk structures. Surfaces (101) and (210) have been exposed for anatase and brookite, respectively. For each compound, the non–crystallographic direction (Z) has been chosen to lie orthogonal to either plane, that is, along [101] and [210] directions in the corresponding crystallographic reference systems. The slab depth of anatase (brookite) has been set to 5 (3) TiO_2 layers along Z, to have a reasonable trade-off among the desired variational flexibility and the complexity of the simulation box. The primitive surface mesh of anatase has cell parameters a_1= 3.78 Å, a_2 =5.53 Å and γ = 69.2 deg. The brookite primitive mesh is larger, with a_1= 5.15 Å, a_2 =8.16 Å and γ = 60.8 deg (Figure S5), even though the general shape of the two 2D cells is very similar. Each basic mesh has been replicated along the corresponding crystallographic directions a_1(X) (anatase: 4 times; brookite: 2 times) and a_2 (Y) (anatase: 2 times; brookite: 2 times) to generate 2D–periodic slabs with approximately the same translation–independent surface area.
The next step has been to assemble the interphase model by putting in close contact the (101) surface of anatase with the (210) one of brookite along the non–periodic Z direction. Due to the complexity of the system, numerical divergences are probable, especially if the starting configuration is too far from a true potential energy minimum. Moreover, quantum simulations require a significant amount of computational resources. To dispose of hard contacts and chemically unfavourable coordination geometries of Ti atoms in the interfacial region, the 1x1 surface mesh of brookite has been oriented to fit as much as possible the 2x1 one of anatase. Indeed, cell parameters of the 2x1 anatase mesh are almost commensurate with the brookite ones: $2\cdot a_1$(anatase)=7.56 Å; ratios of the mesh edges are a_2(brookite)/$2\cdot a_1$(anatase)=1.08 and a_2(anatase)/a_1(brookite) = 1.07. Thus, a reasonable starting point can be obtained if the brookite mesh is rotated around Z so that a_2(brookite) is roughly parallel to $2\cdot a_1$(anatase), and a_1(brookite) is oriented as a_2(anatase) (Figure S5). Eventually, the whole translation–independent part of the slab consists of repetitions of 4x2

(anatase side) and 2x2 (brookite side) unit cells. This allows to superimpose the 1x1 surface mesh of brookite with the 2x1 anatase mesh, allowing almost commensurate matching.
As full 3D periodicity is always exploited in quantum simulations, a 12 Å wide layer of vacuum has been added along the non–crystallographic Z direction. This is enough to avoid any relevant interaction among translation–related replicas of the slab model. Eventually, this consists of a 3 nm thick anatase/brookite biphasic system with 384 atoms.
Atom layers of both phases lying farthest from the interphase region have been kept frozen at their bulk geometries, as estimated from DFT optimizations of the individual semiconductors. All other atoms in the system have been relaxed at constant volume of the simulation box, without imposing any symmetry constraint. Due to the large dimensions of the simulation box, only the Γ point of the first Brillouin zone has been considered to solve the SCF equations. As detailed above in Section S2.1, other computational parameters have been kept identical to those employed for simulations of isolated phases.

Supplementary Figure 5
Matching of the surface meshes of anatase and brookite and their correlation with the starting model of the biphasic slab. The red box on the left is the view along Z of the anatase (101) mesh. Cell edge lengths are expressed in Å. The gold box shows the analogue view for the brookite (210) mesh. The blue box on the right displays how the interphase has been built: the brookite slab has been rotated through a visual procedure implemented in Diamond v3.2k ((c) 1999–2014 Crystal Impact GbR, Bonn Germany), until the (210) mesh has been superimposed almost exactly to the 2x1 (101) mesh of anatase (see text). The outcome, which has been employed as the starting configuration for the quantum mechanical optimization, is shown in the black inset.

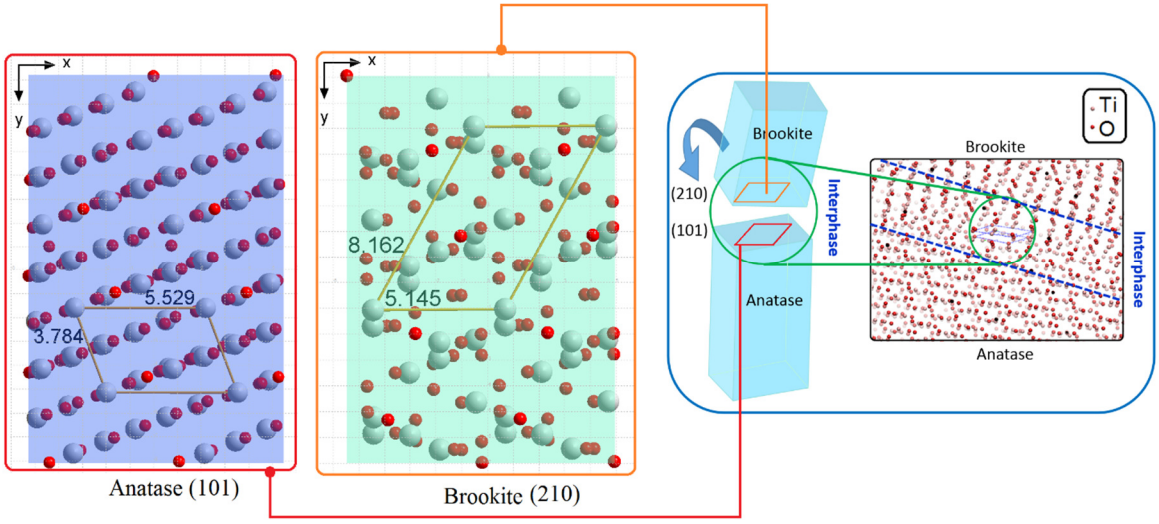

S3.4 Geometry changes after optimization

Supplementary Figure 6.
Average Root Mean Square Deviation (RMSD) per layer along the non–crystallographic z–coordinate (rumpling function) with respect to the starting point of the simulation (bulk structures). The reference zero is set at the interphase; distances are negative in the anatase region and positive in the brookite one. In both phases, lighter O atoms (red line and filled circle) are more extensively rearranged than heavier Ti atoms (blue line and filled circle). The amount of rearrangement is quite consistent. Nevertheless, the suitable mesh matching described above provides a guess enough educated to reach nuclear minimum convergence is a feasible amount of time. Anatase undergoes the most significant geometric changes, reaching a depth of 1 nm from the interphase, while the bulk brookite structure is unperturbed already at 0.4 nm from the interphase. This also proves that the selected slab depths for the two phases (see above) are large enough to describe all the relevant rearrangements that take place at the interphase.

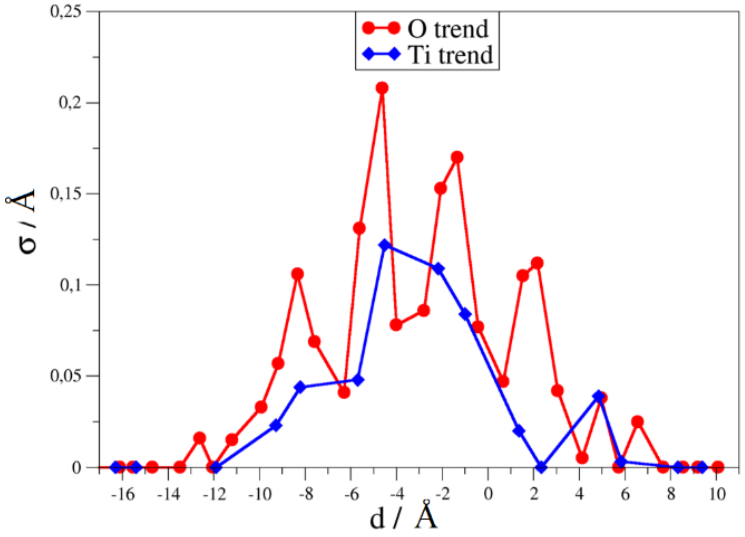

Supplementary Figure 7.
Starting (transparent) and final optimization (dense) geometries of the mixed anatase/brookite supercell. Brookite geometry is almost preserved, while anatase one is significantly changed. Border layers geometries are frozen. The interphase geometry is significantly different from both phases. In the junction region, several new Ti–O bonds have been formed (see also Figure S8), indicating that important structural effects occur at the interphase between anatase and brookite.

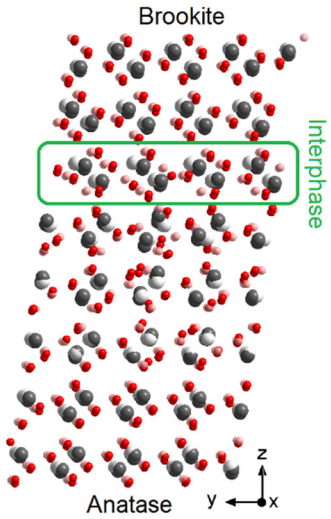

Supplementary Figure 8.
Focus on the interphase region for the starting and final optimization steps of the mixed anatase/brookite supercell.

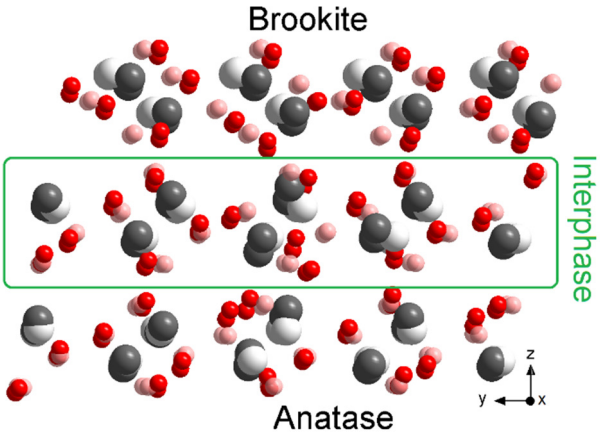

S3.5 Partial Density of State calculation for Anatase, Brookite and Interphase atoms

Supplementary Figure 9.
Partial Density of States (PDOS) for titanium atoms (panel (a)) and oxygen atoms (panel(b)) at different layer level. From bottom to top, PDOS for anatase deep layers (black lines), for anatase at the interphase region (red line), brookite atoms at the interphase (green line), and brookite deep layers (blue lines). From a qualitative point of view, the inter–layer DOS are more similar to the brookite than the anatase phase ones. This is in agreement with the fact that at the interphase the original anatase geometry is significantly changed, while the brookite one is almost preserved. The Zero in Energy has been set equal to the Fermi Energy. The Ti and O PDOS at the interphase are shifted about 0.7eV at higher energies, if compared with both the anatase and brookite bulk ones. In conclusions, the interphase DOS is different from both the bulk anatase and brookite one and cannot be reproduced by a simple alignment. Vertical dashed lines indicate the band gap region.

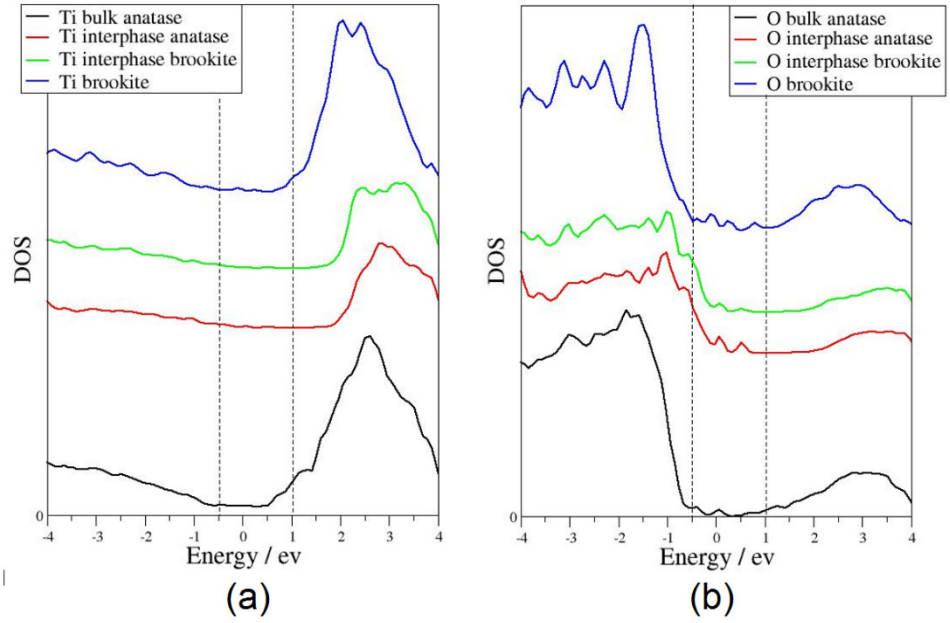

S3.6 The interphase capacity: QTAIM partial charges calculation

Atomic charges are calculated by means of Quantum Theory of Atoms in Molecules (QTAIM),[20] taking advantage of the algorithm of Henkelman.[21] Bader atomic charges in the anatase polymorph are positive, while in brookite negative for a total of 0.5 electrons (see Figure S10 SI). Considering that the optimized modules of the simulation box vectors are X =10.42 Å, Y =14.12 Å and Z=39.92 Å, the translation–independent part of the interphase plane has area $1.47 \cdot 10^{-14}$ cm^2. The specific charge transfer amounts thus to 5.4 $\mu C \cdot cm^{-2}$.

Supplementary Figure 10.
(a) Average QTAIM net atomic charges, of Ti (blue) (<q(Ti)>) and O (red) (<q(O)>) atoms in the composite anatase/brookite slab model, as a function of the layer number (b) along the non–crystallographic direction Z. Vertical bars correspond to 1 estimated standard deviations of the mean and should be interpreted as a measure of the dispersion of individual charges in each layer. The numerical integration error amounts to $-1.3 \cdot 10^{-3}$ charge units in the whole simulation box. Layers are spaced by steps of ~ 3.8 Å for anatase and ~ 3.5 Å for brookite and bear $Ti_{16}O_{32}$ translation–independent clusters each. "0" marks the interphase center of mass. Layers –3 (brookite side) and 5 (anatase side) confine with vacuum: atoms in these layers have been kept frozen at their experimental estimates (see text). This choice is motivated by the necessity of introducing the information of the bulk structure into our model, which consists of three phases (anatase, brookite, vacuum) roughly 1 nm thick each, while real nanoparticles have average dimensions of ~ 7 nm at least. Thus, surface atoms in contact with the vacuum are at fixed bulk geometry and undercoordinated. The charge effects induced by these constrains are quite contained (anatase side: ~ +0.05 e for O and ~ –0.08 e for Ti; Brookite side: ~ +0.02 e for O and –0.02 e for Ti). Since these charge displacements are small, we avoid a full slab optimization that would have jeopardized the interphase electronic structure and the net charge difference calculation. (c) Pictorial representation of total Bader net charges of Ti (blue) and O (red) across the slab model. Lighter colors correspond to oxidized atoms (i.e., larger net positive charges on Ti and less negative net charges on O). Darker colors mean reduced atoms (i.e. lower net positive charges on Ti and more negative net charges on O). Ti atoms charges range from +1.7 to +2.2 *e*. O atom charges range form –0.7 to –1.1 *e*. The total charges of layers from nº –3 to –1 and from nº +1 to +5 (see panel (b)) are respectively –0.5 and +0.5 *e*, in agreement with layer–based estimates. Overall, we predict that an equilibrium net charge transfer occurs from the anatase to the brookite side.

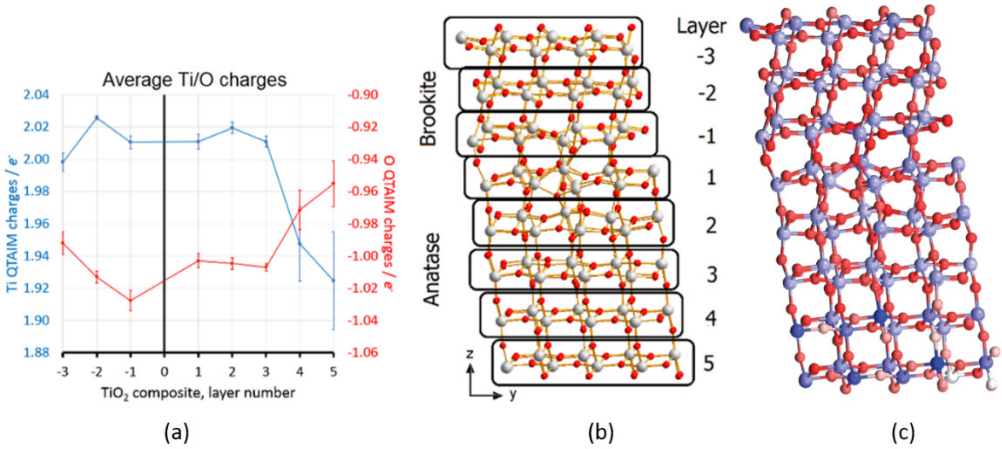

Supplementary Table 1

Coordinates (Å) of Ti ions in the anatase:brookite heterostructure corresponding to the optimized DFT geometries and net atomic charges, as computed by the QTAIM method. See Figure S10 for numbering of layers (negative index: brookite; positive index: anatase).

Layer	X	Y	Z	q(Ti)	Layer	X	Y	Z	q(Ti)
-3	4.2830	2.1732	25.3105	2.0147	2	3.0043	-1.3619	11.3129	2.022
-3	9.4908	2.0684	25.1792	2.0181	2	4.1873	2.1155	11.2722	2.0029
-3	0.2734	-1.3112	25.4408	2.0243	2	5.6889	5.5637	11.2460	1.9966
-3	0.2077	9.3140	25.4390	2.0043	2	0.5055	5.6547	11.5305	2.0081
-3	5.4812	-1.4159	25.3093	2.0267	2	6.6751	9.0965	11.2321	2.0153
-3	5.4154	9.2093	25.3075	1.9755	2	1.4916	9.1648	11.3821	2.0188
-3	4.2597	5.6677	25.3658	2.0188	2	8.2201	-1.4351	11.2407	2.0204
-3	9.4675	5.5629	25.2344	2.0235	2	9.4045	2.0613	11.1918	2.0221
-3	2.8602	-3.6088	26.3897	1.9577	2	1.5852	1.0889	12.5567	2.0186
-3	8.0680	-3.7135	26.2584	1.9796	2	3.1578	4.5083	12.8063	2.0481
-3	1.6388	3.4748	26.4459	2.0124	2	4.1089	8.0268	12.3737	2.0206
-3	6.8464	3.3700	26.3147	2.0065	2	5.4302	11.6153	12.3032	2.0327
-3	2.8369	-0.1142	26.4447	1.9723	2	0.2576	11.6886	12.4996	2.0047
-3	8.0447	-0.2190	26.3136	1.976	2	6.7838	1.0321	12.3585	2.019
-3	1.6154	6.9693	26.5012	1.9754	2	8.3575	4.4614	12.6770	2.0424
-3	6.8231	6.8646	26.3699	1.9854	2	9.3119	7.9917	12.2490	2.0198
-2	4.279	-2.000	21.782	2.0239	3	1.7619	-0.9991	7.7371	2.0091
-2	9.486	-2.066	21.640	2.0244	3	3.1078	2.5068	7.7222	2.0152
-2	0.319	5.137	21.920	2.0277	3	4.3790	6.0153	7.6762	2.0226
-2	5.531	5.068	21.762	2.0269	3	5.6346	9.5581	7.6602	2.0256
-2	4.265	1.497	21.912	2.0178	3	0.3797	9.5994	7.8892	1.9983
-2	9.475	1.424	21.779	2.0218	3	7.0623	-1.0857	7.7001	1.9967
-2	0.212	8.615	22.062	2.0286	3	8.4397	2.4184	7.6054	2.0072
-2	5.424	8.542	21.912	2.0252	3	9.7293	5.8555	7.7495	1.9697
-2	1.707	-0.805	22.872	2.0338	3	0.5726	1.4778	8.9727	2.007
-2	6.903	-0.879	22.722	2.0316	3	1.8662	4.9492	8.9571	2.0139
-2	2.903	6.264	22.877	2.0256	3	3.0008	8.5023	8.7795	2.0179
-2	8.109	6.193	22.746	2.0244	3	4.1881	12.0352	8.7053	2.0272
-2	1.685	2.693	22.941	2.0327	3	5.7471	1.4373	8.7355	2.0145
-2	6.893	2.616	22.802	2.0292	3	7.0133	4.9113	8.7399	2.0108
-2	2.820	9.741	22.950	2.0205	3	8.2209	8.4012	8.7062	2.0245
-2	8.021	9.671	22.802	2.0174	3	9.4640	11.9267	8.6717	2.0149
-1	0.2318	0.8721	18.5071	2.0171	4	0.3746	-0.5282	4.2746	1.8396
-1	5.4436	0.8084	18.3526	2.0168	4	1.6856	2.9609	4.2470	1.9593
-1	4.1986	-2.7434	18.3203	2.0297	4	2.9965	6.4500	4.2194	2.0237
-1	4.0447	7.8947	18.4696	1.9775	4	4.3074	9.9391	4.1918	2.0246
-1	9.4046	-2.8167	18.1893	2.0344	4	5.9674	-0.5945	4.2108	2.0178

Layer	X	Y	Z	q(Ti)	Layer	X	Y	Z	q(Ti)
-1	9.2539	7.8228	18.3350	1.9831	4	7.2784	2.8946	4.1833	2.0231
-1	0.4341	4.3566	18.4294	2.0035	4	8.5893	6.3837	4.1557	1.9381
-1	5.6992	4.2935	18.2285	1.9933	4	9.9002	9.8728	4.1281	1.7629
-1	2.8981	1.9331	19.3555	2.0094	4	0.2148	5.5061	5.1720	1.7803
-1	8.1085	1.8568	19.2276	2.0109	4	1.5257	8.9952	5.1444	1.9373
-1	1.6314	-1.6387	19.4522	2.0172	4	2.8366	12.4842	5.1168	2.0215
-1	1.4802	9.0083	19.4249	2.0215	4	10.0219	1.8322	4.9792	1.8271
-1	6.8384	-1.7144	19.2971	2.017	4	4.4966	1.9506	5.1359	2.0063
-1	6.6868	8.9310	19.2733	2.023	4	5.8075	5.4397	5.1083	2.0082
-1	2.9729	5.3689	19.3930	2.0086	4	7.1185	8.9288	5.0807	2.0195
-1	8.1934	5.3009	19.2669	2.0061	4	8.4294	12.4179	5.0531	1.9711
1	4.0914	-1.7295	14.8358	2.0243	5	0.4511	3.4846	0.7773	1.8348
1	5.2263	1.9827	14.8821	2.0403	5	1.7620	6.9737	0.7498	1.9231
1	0.0167	2.0539	15.0904	2.0413	5	3.0729	10.4628	0.7221	2.1924
1	5.8258	5.2584	14.5006	2.0006	5	10.2582	-0.1893	0.5846	1.7243
1	0.7234	5.2798	14.8318	2.0011	5	4.7329	-0.0708	0.7412	1.972
1	7.8402	8.6971	14.8154	2.0103	5	6.0439	3.4183	0.7136	1.9993
1	2.6515	8.7767	14.9477	2.0177	5	7.3548	6.9074	0.6860	1.9826
1	9.2972	-1.8043	14.7396	2.0044	5	8.6657	10.3965	0.6584	1.8046
1	2.7214	0.7843	16.0143	2.0192	5	0.2912	9.5188	1.6748	1.7157
1	3.4996	4.4248	16.3338	1.9867	5	1.6021	13.0079	1.6472	1.9451
1	5.2606	7.7766	15.8911	1.982	5	8.7874	2.3559	1.5096	1.9246
1	0.0571	7.8820	16.0395	1.9846	5	3.2621	2.4743	1.6663	1.9861
1	6.5366	11.2954	15.8384	2.0226	5	10.0983	5.8450	1.4821	1.8082
1	1.3525	11.3757	16.0000	2.022	5	4.5730	5.9634	1.6387	1.9824
1	7.8981	0.7042	15.8643	2.0225	5	5.8840	9.4525	1.6111	1.9963
1	8.6774	4.3472	16.0185	1.9943	5	7.1949	12.9416	1.5835	2.0017

Supplementary Table 2

Coordinates (Å) of O ions in the anatase:brookite heterostructure corresponding to the optimized DFT geometries and net atomic charges, as computed by the QTAIM method. See Figure S10 for numbering of layers (negative index: brookite; positive index: anatase).

Layer	X	Y	Z	q(O)	Layer	X	Y	Z	q(O)
-3	1.9581	-0.4293	24.7653	-0.9686	2	0.6185	1.2702	10.9124	-0.9887
-3	7.1571	-0.5397	24.6017	-0.9673	2	2.2654	5.1089	10.8965	-1.0213
-3	2.6131	6.6106	24.7420	-0.9744	2	3.0941	8.1953	10.7258	-0.9981
-3	7.8209	6.5059	24.6107	-0.9688	2	4.5780	12.1296	10.6202	-1.0255
-3	4.5260	0.3591	25.3923	-0.9902	2	5.8760	1.2805	10.6709	-0.9967
-3	-0.6819	0.3901	25.5488	-0.9897	2	7.4112	4.9225	10.6299	-0.9966
-3	-0.0181	7.5094	25.5326	-0.9888	2	8.2735	8.0903	10.6339	-1.0004
-3	5.1895	7.4047	25.4013	-0.9936	2	9.8154	12.0933	10.5626	-1.0167
-3	2.5940	1.6998	26.3631	-1.0068	2	3.0883	0.5358	11.2518	-1.0055
-3	7.8017	1.5951	26.2317	-1.0086	2	4.6270	3.9798	11.4605	-1.0060
-3	1.8413	8.7738	26.4075	-1.0027	2	5.5877	7.5003	11.1759	-0.9959
-3	7.0489	8.6691	26.2762	-0.9843	2	0.3975	7.5801	11.3317	-1.0041
-3	-0.8924	9.6736	27.1378	-0.9684	2	7.1499	10.9515	11.5707	-1.0259
-3	-0.0373	2.5987	27.1536	-0.9181	2	1.9520	11.0257	11.7010	-1.0289
-3	5.1704	2.4939	27.0222	-0.9369	2	8.3210	0.4641	11.1367	-1.0088
-3	4.4177	9.5679	27.0667	-0.8899	2	9.8816	3.9093	11.4313	-0.9999
-3	0.8374	2.9032	24.7652	-0.9984	2	1.5129	-0.8182	12.5785	-0.9954
-3	6.0556	2.8296	24.6240	-0.9966	2	2.5623	2.7748	12.2835	-1.0103
-3	3.5845	9.9156	24.7123	-0.9966	2	4.3017	6.1171	12.8266	-1.0629
-3	8.7983	9.8439	24.5370	-0.9977	2	4.9616	9.7530	12.0157	-1.0171
-3	1.1455	-3.0272	25.6857	-1.0374	2	-0.2207	9.8342	12.1643	-1.0185
-3	6.3532	-3.1319	25.5543	-1.0470	2	6.6760	-0.8786	12.3814	-0.9947
-3	3.3923	3.9866	25.6546	-1.0347	2	7.7648	2.7194	12.1443	-1.0061
-3	8.6002	3.8818	25.5231	-1.0338	2	9.4472	6.0925	12.6369	-1.0444
-3	3.7275	-1.9277	26.1008	-1.0607	2	4.0290	-1.5156	12.9498	-0.9911
-3	8.9353	-2.0325	25.9695	-1.0512	2	4.9811	1.4983	12.9692	-0.9797
-3	0.7667	5.1909	26.2010	-1.0470	2	-0.2195	1.6045	13.1899	-0.9813
-3	5.9744	5.0861	26.0697	-1.0552	2	6.7751	5.6022	12.8370	-0.9588
-3	1.0865	-0.7247	27.1519	-0.9634	2	1.5590	5.6151	13.1182	-0.9702
-3	6.2942	-0.8294	27.0206	-0.9463	2	7.4942	8.5258	12.9371	-1.0142
-3	3.3333	6.2892	27.1207	-0.9697	2	2.2943	8.5561	13.0657	-1.0167
-3	8.5411	6.1843	26.9893	-0.9542	2	9.2382	-1.5848	12.8603	-0.9711
-2	2.6390	2.4173	21.2148	-1.0079	3	0.8689	5.1798	7.2961	-0.9992
-2	7.8375	2.3208	21.0886	-0.9991	3	1.9939	8.9260	7.0573	-1.0172
-2	1.8344	9.4241	21.2689	-0.9952	3	3.2297	12.3525	7.0278	-1.0135
-2	7.0329	9.3581	21.1130	-0.9929	3	-0.2118	1.8708	7.2702	-1.0352
-2	0.0274	3.2447	22.0076	-0.9830	3	4.8209	1.8624	7.0420	-1.0048

Layer	X	Y	Z	q(O)	Layer	X	Y	Z	q(O)
-2	5.2402	3.1762	21.8593	-0.9844	3	6.0661	5.3208	7.0087	-0.9960
-2	4.4175	10.2366	21.8788	-0.9885	3	7.3713	8.8790	7.0122	-1.0190
-2	9.6258	10.1716	21.7322	-0.9877	3	8.5973	12.3137	6.9865	-1.0054
-2	2.6778	-2.4945	22.8832	-0.9941	3	2.2285	0.8214	8.0024	-1.0159
-2	7.8800	-2.5662	22.7214	-0.9950	3	3.4189	4.3734	7.8545	-0.9899
-2	1.9586	4.5798	22.9031	-0.9870	3	4.6942	7.8973	7.9010	-1.0191
-2	7.1688	4.5044	22.7465	-0.9885	3	5.7917	11.4513	7.6463	-1.0015
-2	0.0522	-1.6298	23.5835	-0.9915	3	0.5776	11.4742	7.8124	-1.0033
-2	5.2485	-1.7034	23.4414	-0.9944	3	7.4721	0.7602	7.9092	-1.0302
-2	4.5658	5.3761	23.4947	-1.0067	3	8.6047	4.3379	7.6586	-0.9996
-2	-0.6387	5.4375	23.6510	-1.0037	3	9.9410	7.7796	7.8222	-1.0198
-2	0.8086	-1.4389	21.2169	-1.0133	3	0.1653	-0.3841	8.7539	-1.0061
-2	6.0088	-1.5126	21.0622	-1.0134	3	1.6406	3.0561	9.0013	-1.0034
-2	3.8029	5.6031	21.1141	-1.0339	3	2.6735	6.6585	8.5649	-1.0041
-2	9.0105	5.5483	20.9916	-1.0326	3	4.0132	10.1276	8.7324	-1.0075
-2	3.3754	-0.2276	22.0779	-1.0289	3	5.3477	-0.4266	8.4928	-1.0132
-2	8.5841	-0.2991	21.9483	-1.0297	3	6.7661	3.0267	8.6008	-1.0088
-2	1.1805	6.8845	22.1835	-1.0247	3	7.9306	6.5648	8.4554	-1.0088
-2	6.3904	6.8126	22.0375	-1.0245	3	9.2597	10.0242	8.7565	-1.0094
-2	0.7896	0.9380	22.7450	-1.0420	3	2.6309	-1.5399	9.4300	-1.0143
-2	5.9872	0.8667	22.5968	-1.0400	3	4.1051	2.2639	9.3685	-0.9668
-2	3.7520	7.9833	22.7119	-1.0360	3	5.2855	5.5740	9.3638	-1.0069
-2	8.9560	7.9105	22.5632	-1.0360	3	0.1049	5.5549	9.6584	-0.9924
-2	3.3820	2.0782	23.5924	-1.0390	3	6.6039	9.3675	9.3375	-1.0048
-2	8.5902	1.9960	23.4628	-1.0416	3	1.4239	9.4648	9.4745	-0.9928
-2	1.1068	9.1940	23.7032	-1.0367	3	7.8674	-1.6600	9.3503	-1.0128
-2	6.3144	9.1052	23.5560	-1.0448	3	9.3571	2.2763	9.2909	-1.0011
-1	2.4485	-2.1604	17.7098	-1.0433	4	0.5513	9.3914	3.5673	-0.8139
-1	7.6566	-2.2413	17.5587	-1.0479	4	1.8622	12.8805	3.5397	-0.9747
-1	2.1130	5.0830	17.6195	-1.0445	4	9.0475	2.2285	3.4021	-1.0114
-1	7.4125	4.9578	17.4585	-1.0578	4	3.5222	2.3469	3.5587	-1.0095
-1	-0.0180	-1.0108	18.6183	-0.9881	4	-0.0572	5.8534	3.6625	-0.8662
-1	5.1914	-1.0790	18.4660	-0.9854	4	4.8332	5.8360	3.5312	-1.0127
-1	4.4916	5.9233	18.2557	-1.0765	4	6.1441	9.3251	3.5036	-1.0049
-1	9.7328	5.8798	18.2004	-1.0543	4	7.4550	12.8143	3.4760	-1.0191
-1	1.8766	0.2765	19.4756	-1.0068	4	0.6730	1.3508	4.4184	-0.8363
-1	7.0818	0.2008	19.3213	-1.0049	4	1.9839	4.8400	4.3909	-0.9802
-1	2.5087	7.2562	19.4247	-1.0019	4	3.2948	8.3290	4.3633	-1.0138
-1	7.7107	7.1911	19.2854	-1.0035	4	4.6057	11.8181	4.3357	-1.0384
-1	4.5785	1.1845	20.0669	-0.9852	4	6.2658	1.2845	4.3548	-1.0144
-1	9.7804	1.0857	19.9375	-0.9883	4	7.5767	4.7736	4.3272	-1.0246
-1	-0.1546	8.2142	20.2433	-0.9843	4	8.8876	8.2627	4.2996	-1.0001

Layer	X	Y	Z	q(O)	Layer	X	Y	Z	q(O)
-1	5.0504	8.1311	20.0912	-0.9888	4	-0.2171	11.8876	4.5599	-0.9800
-1	3.6009	0.9342	17.7795	-1.0385	4	-0.0836	3.6270	5.0281	-0.9356
-1	8.8135	0.8990	17.6329	-1.0308	4	1.2273	7.1161	5.0005	-1.0088
-1	0.6207	8.1689	17.8863	-0.9908	4	2.5383	10.6052	4.9729	-1.0105
-1	5.8329	8.0742	17.7354	-0.9933	4	9.7236	-0.0468	4.8354	-0.8240
-1	1.1917	2.6374	18.8021	-1.0239	4	4.1983	0.0716	4.9920	-1.0252
-1	6.4117	2.5691	18.6428	-1.0187	4	5.5092	3.5607	4.9644	-1.0145
-1	3.1613	9.6437	18.7071	-1.0235	4	6.8201	7.0498	4.9368	-1.0098
-1	8.3708	9.5751	18.5700	-1.0245	4	8.1311	10.5389	4.9092	-0.9841
-1	0.5003	10.7028	19.1897	-1.0602	4	1.3490	-0.9245	5.8517	-0.9978
-1	5.7024	10.6272	19.0250	-1.0628	4	2.6599	2.5646	5.8241	-1.0384
-1	3.8640	3.5925	18.7823	-1.1190	4	3.9709	6.0537	5.7965	-1.0046
-1	9.0964	3.5276	18.8131	-1.0999	4	5.2818	9.5428	5.7689	-1.0074
-1	3.3949	-2.1426	20.0665	-1.0215	4	-0.2435	9.6612	5.9256	-0.8723
-1	8.6004	-2.2049	19.9247	-1.0181	4	6.9418	-0.9908	5.7880	-0.9651
-1	1.2349	4.9410	20.1508	-1.0443	4	8.2527	2.4983	5.7604	-0.9733
-1	6.4245	4.8862	19.9802	-1.0524	4	9.5637	5.9874	5.7328	-0.8159
1	1.8144	1.4839	14.4523	-0.9994	5	2.2202	2.8185	-0.0038	-0.9557
1	2.3570	4.2819	14.8496	-0.9766	5	3.5311	6.3076	-0.0314	-0.9363
1	4.4607	8.4378	14.2568	-0.9947	5	4.8421	9.7967	-0.0590	-0.9069
1	5.5339	11.4448	14.2093	-0.9831	5	6.1530	13.2858	-0.0866	-0.9332
1	0.3213	11.5055	14.3908	-0.9559	5	0.6277	13.4042	0.0701	-0.7140
1	7.0127	1.3704	14.2698	-0.9944	5	7.8130	2.7522	-0.0675	-0.9956
1	7.4830	4.2383	14.5793	-0.9614	5	9.1239	6.2413	-0.0951	-0.9924
1	9.6650	8.3929	14.1304	-0.9977	5	0.0193	9.8662	0.1646	-0.8951
1	4.4035	0.1921	15.1123	-1.0061	5	0.7494	5.3636	0.9213	-0.8401
1	4.7304	3.7838	13.9841	-1.0130	5	2.0603	8.8527	0.8937	-0.9221
1	9.8875	3.7904	13.9621	-1.0253	5	3.3712	12.3418	0.8661	-1.0086
1	6.7659	6.9463	15.0865	-1.0230	5	0.1409	1.8255	1.0164	-0.9524
1	1.5746	7.0357	15.2677	-1.0185	5	5.0312	1.8082	0.8851	-1.0203
1	8.0958	10.6411	14.7769	-1.0009	5	6.3422	5.2973	0.8575	-1.0360
1	2.8847	10.7179	14.8761	-1.0032	5	7.6531	8.7864	0.8300	-1.0569
1	9.6124	0.1188	15.0212	-1.0048	5	8.9640	12.2755	0.8023	-1.0598
1	2.3364	-1.0478	15.4652	-1.0086	5	-0.0072	7.6398	1.5309	-0.9354
1	3.6438	2.4961	15.9410	-0.9499	5	1.3038	11.1289	1.5033	-0.9767
1	4.3481	6.0257	15.5517	-1.0114	5	8.4891	0.4769	1.3657	-1.0197
1	9.6027	5.9738	15.4568	-1.0184	5	2.9638	0.5953	1.5224	-1.0492
1	6.3182	9.4081	15.8056	-0.9771	5	9.8000	3.9659	1.3382	-0.8227
1	1.1422	9.4893	15.9603	-0.9780	5	4.2747	4.0844	1.4948	-1.0091
1	7.5281	-1.1240	15.3233	-1.0077	5	5.5856	7.5735	1.4672	-1.0235
1	8.7742	2.4267	15.7796	-0.9739	5	6.8965	11.0626	1.4396	-1.0261
1	4.9065	-2.5300	16.5196	-1.0333	5	-0.0769	13.7198	2.3749	-0.8265

Layer	X	Y	Z	q(O)	Layer	X	Y	Z	q(O)
1	-0.2804	-2.4737	16.6884	-1.0280	5	1.4254	3.0883	2.3545	-0.9967
1	0.2140	3.9818	16.5455	-1.0554	5	2.7364	6.5774	2.3269	-0.9941
1	5.4612	3.9790	16.3543	-1.0393	5	4.0473	10.0665	2.2993	-0.9400
1	0.9803	1.2083	16.7510	-1.0231	5	5.7073	-0.4671	2.3184	-0.9649
1	6.1678	1.1420	16.5896	-1.0244	5	7.0182	3.0220	2.2908	-0.9748
1	3.5143	8.2485	16.6318	-1.0045	5	8.3291	6.5111	2.2632	-0.9557
1	8.7094	8.1616	16.4985	-1.0059	5	9.6401	10.0002	2.2356	-0.8212

S3.7 The plane-averaged electrostatic potential

A lot of physical insights into the anatase/brookite composite slab presented above can be obtained by calculating the plane-averaged electrostatic potential along the direction crossing the two phases, which we denominate Z. This potential, $\bar{V}$, is obtained from the averaged of the potential part of the electronic Hamiltonian over the ground state electronic wavefunction at fixed z after the averaged over the x-y perpendicular plane values. We performed this calculation with the PBE+U computational set-up described above and also at the level of HSE06 functional theory by employing the PBE+U optimized slab geometry. The results are reported in Fig. S11 below in panel (b) and panel (a), respectively for the two functionals. The continuous black line is for the potential itself, while the averaged electrostatic potential is reported as a continuous red line. On the upper part of the figure, a portion of the slab is also reported to guide the eye along each layer.
The plane-averaged electrostatic potential profile presents two quasi–plateaus in correspondence of the bulk region of the two polymorphs. The potential difference between these quasi–plateaus is about 0.7eV, where the brookite potential is more negative than the anatase one. By recalling that the plane-averaged electrostatic potential is given by the bracket over the ground electronic state wavefunction of the potential operator part of the electronic Hamiltonian, then the value of the averaged potential is the direct consequence of the electronic distribution. This result represents a confirmation of the charge transfer direction obtained from the Bader's method described above, because it shows once again that the electronic density is slightly higher in the brookite bulk phase respect to the anatase one.

Supplementary Figure 11.

Black solid line (left axis): Calculated plane-averaged electrostatic potential (V); red solid line (right axis): macroscopic average of V for the mixed anatase/brookite system. Panels (a) and (b) are for HSE06 and PBE+U computational set-up respectively. Light blue atoms: Ti; red atoms: O.

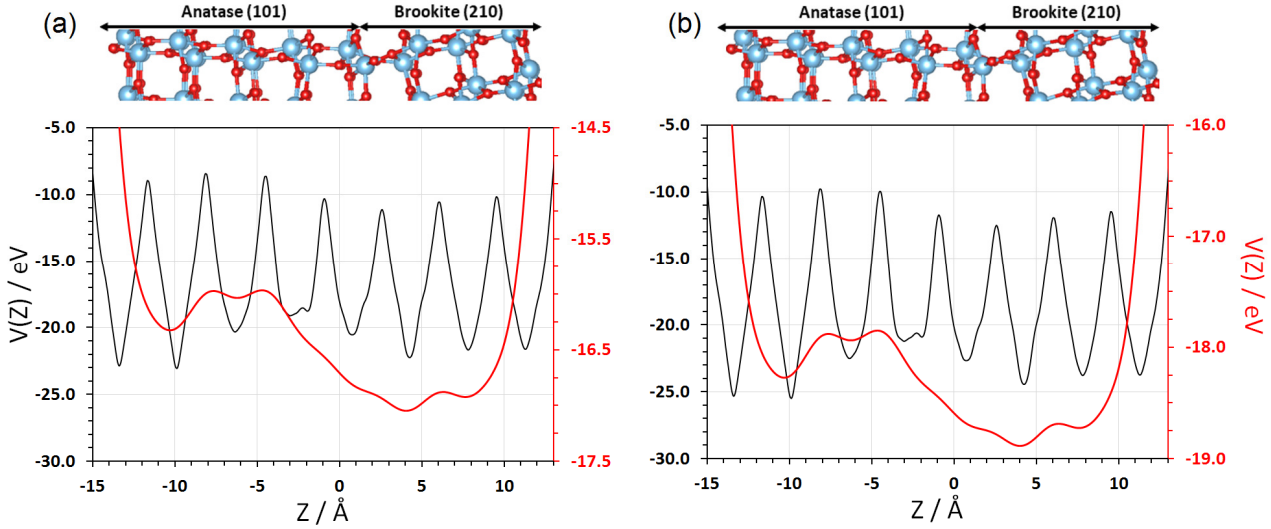

S3.8 Band alignment using the plane-averaged electrostatic potential

The relative position of the band edges of anatase and brookite has been evaluated by using a common reference, which is the calculated plane-averaged electrostatic potential in the composite system and in the separated moieties[22–24]. In this method one starts from the Valence Band Maximum (*VBM*) and the Conduction Band Minimum (C*BM*) of the separated bulk anatase and brookite estimate. Then he obtains their relative positioning in a composite system by aligning these values with respect to the macroscopic averaged electrostatic potential calculated in both separated components and composite system. The Valence Band Offset (VBO) and the Conduction Band Offset (CBO) estimates according to this approach are described in Eq.2 and Eq.3 respectively.[25,26]

$$VBO = (VBM^{bro} - \bar{V}^{bro}) - (VBM^{ana} - \bar{V}^{ana}) + (\bar{V}^{bro,Het} - \bar{V}^{ana,Het}) \quad \text{(Eq. 2)}$$

$$CBO = (CBM^{bro} - \bar{V}^{bro}) - (CBM^{ana} - \bar{V}^{ana}) + (\bar{V}^{bro,Het} - \bar{V}^{ana,Het}) \quad \text{(Eq. 3)}$$

where $\bar{V}^{bro}$ and $\bar{V}^{ana}$ are the reference values from the separated brookite and anatase slabs, and ($\bar{V}^{bro,Het}$) and ($\bar{V}^{ana,Het}$) are the same but evaluated in the composite system, *i.e.* from Figure S11. In this way it is possible to account also for the interface electronic effects. In our case, we set at 0 eV the vacuum level, thus a positive *VBO*/*CBO* indicates that the Valence/Conduction band edge of brookite is higher in energy. If one would use as a reference the standard hydrogen electrode potential (NHE), the same result would imply a sign change of *VBO*/*CBO*. The calculated *VBO* is 0.03 eV, indicating that the valence band edge of brookite is only 0.03 eV above the anatase one. This confirms what seen in figures S2-4 and that the two band edges are almost at the same energy. The Conduction Band Offset (*CBO*) is 0.18 eV, thus 0.15 eV greater that the *VBO*, following that the calculated band gap of brookite (2.69 eV), which is larger than the anatase one (2.54 eV). However, given the well-known deficiencies of the DFT/PBE+U to accurately reproduce the band gap of these semiconductors, we performed the same calculations using the HSE06 hybrid functional, and using the PBE optimized geometry. The calculated band gaps of brookite and anatase are 3.63 eV and 3.46 eV respectively, in close agreement with the experimental values, 3.3 eV and 3.2 eV. As far as the band offset is concerned, HSE06 results corroborate the PBE+U ones, since the calculated *VBO* is -0.02 eV and the *CBO* is 0.20 eV. In conclusions, we find that the CB

edge of anatase is significantly below in energy respect to the brookite one, while the VB edge is very similar in with a type-II alignment as shown in the figure below (Fig.S12). These results are in close agreement with those obtained from quantum mechanical/molecular mechanical (QM/MM) solid-state embedding procedure for anatase and brookite nanoparticles[27] and also to the experimental profiles reported in Figure 6 of Di Paola et al..[28]

Supplementary Figure 12

Band alignment picture of the mixed anatase/brookite system at the level of (a) PBE+U, and (b) HSE06 functionals. Blue regions are for valence band states, and orange regions are for conduction band ones. Light blue atoms: Ti; red atoms: O.

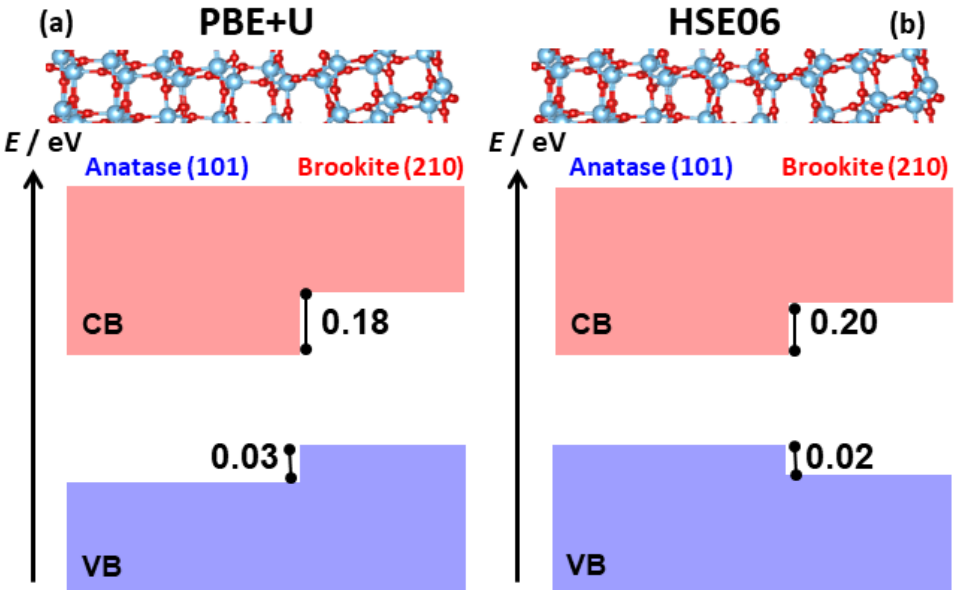

S4. Photocurrent measurements

Supplementary Figure 13
Examples of photocurrent decay at +1V (SCE). Panel (a) for pristine anatase (Alfa Aesar 130) and panel (b) for mixed anatase/brookite (TN_0.4) titania samples. This sample has been chosen due to the low amount of brookite, to see whether even a low nominal brookite amount is enough to cause a significant delay of recombination time. Explanation of the sample labels is given in the Supplementary Table S3. In panel (a) (black line) the value of the generated photocurrent is larger with respect to the mixed anatase/brookite one in panel (b) (green line), because the pristine suspension is more homogeneous and less deposited. The different decay trend is reproducible for each set of pristine anatase and anatase/brookite mixed samples.

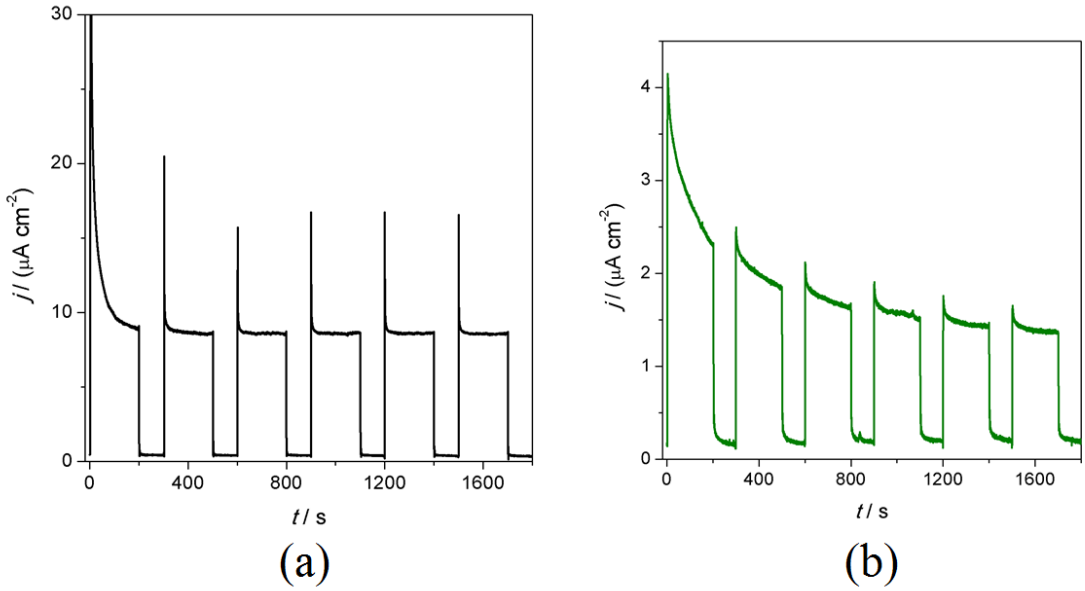

Supplementary Figure 14

Comparison between different decay mechanisms. In panel (a) direct comparison between the normalized current decays previously reported in Figure S13 (a) and (b). Panel (b) shows the photocurrent decay for the first 15s (4th step of irradiation) and the corresponding exponential fittings. Two different exponential decay mechanisms are necessary to properly fit the Alfa Aesar 130 curve (black dots), especially in the range 0–3 seconds. A single decay mechanism describes the TN_0.4 (green dots) data in panel (b). Decays are similar at longer times, *i.e.* after 3 seconds.

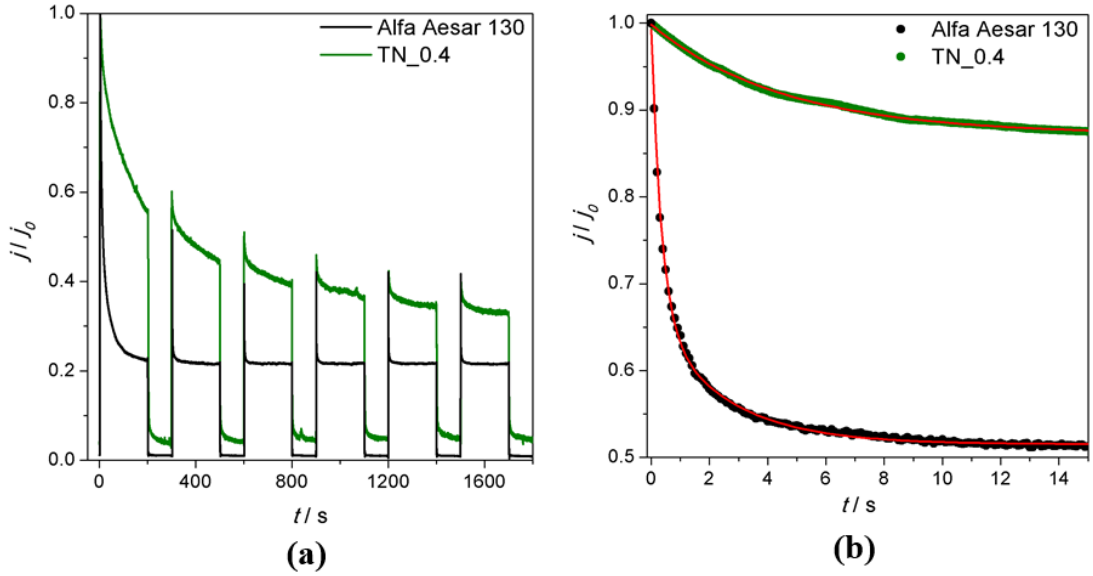

Supplementary Figure 15

BET isotherms (Figure S15a), Diffuse Reflectance spectra (Figure S15b) and X-ray powder diffraction patterns (Figure S15c) of Alpha Aesar 284 and T samples, representative of pure anatase and mixed anatase/brookite nanopowders.

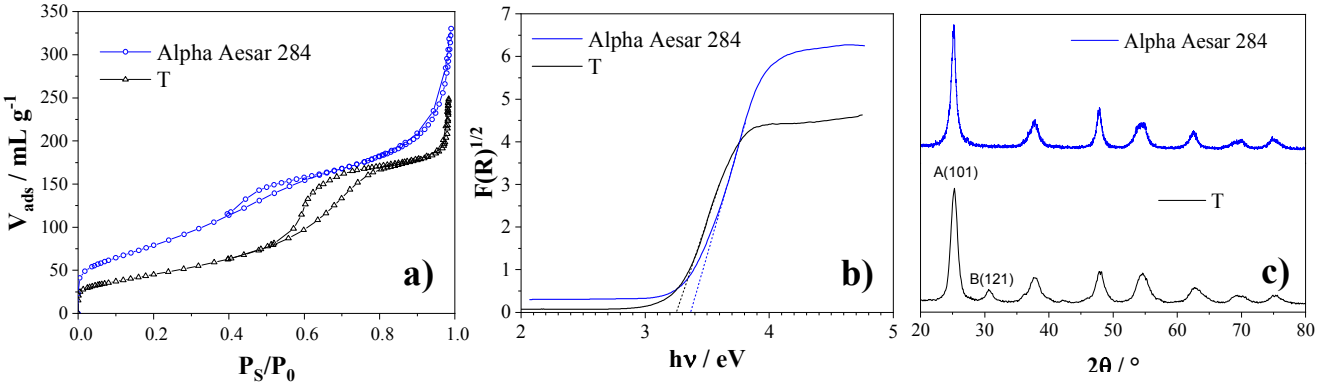

S5. Photocatalysis

Supplementary Table 3

See Section S1 for a detailed description of the experimental setup. Photocatalytic activity under simulated solar irradiation of representative N-doped mixed titania/brookite samples,[29] compared with undoped reference powders containing only anatase. The pollutant disappearance follows a pseudo–first order kinetics; available rate constants refer to the first 40 (κ^{40}) or 140 (κ^{140}) min of the experiment.

Sample	Photocatalytic activity (300W solar lamp, 380–600 nm, I = 1.2×10^{-5} Einstein dm^{-3} s^{-1})			
	Methylene Blue[a]	NO_x[a]	Toluene[b]	
	% mineralization[c]	$\kappa^{40}\times10^{2}$ (min^{-1})	% disappearance[d]	$\kappa^{140}\times10^{3}$ (min^{-1})
Alpha Aesar 284	–	–	56	1.8 ± 0.6
Alpha Aesar 130	50	1.96 ± 0.02	–	–
T400	45	2.47 ± 0.06	60	4.8 ± 0.2
TN_0.01[e]	57	2.86 ± 0.07	–	–
TN_0.05[e]	60	3.02 ± 0.09	65	5.0 ± 0.3
TN_0.10[e]	97	3.22 ± 0.05	–	–
TN_0.20[e]	52	2.97 ± 0.08	68	5.2 ± 0.5
TN_0.50[e]	73	2.88 ± 0.02	50	3.1 ± 0.8

[a] Methylene blue and NO_x photodegradation in dry and gaseous conditions, respectively

[b] Photocatalytic removal of gaseous toluene species.

[c] % Molar percent amount of methylene blue by COD analyses for all samples that has been converted to CO_2, water and volatile light hydrocarbons upon completion of the experiment.

[d] Molar percent amount of toluene that has been disappeared in 5 h.

[e] N–doped samples. The number in the label represents the nominal N/Ti ratio.

Supplementary Figure S16

Photocatalytic performances of biphasic TiO_2:N samples as a function on the nominal nitrogen loading. Points corresponding to Alpha Aesar 130 and 284(references) are highlighted. Tabular data in Supplementary Table 3 above. The broken lines serve only as a guide for the eye.

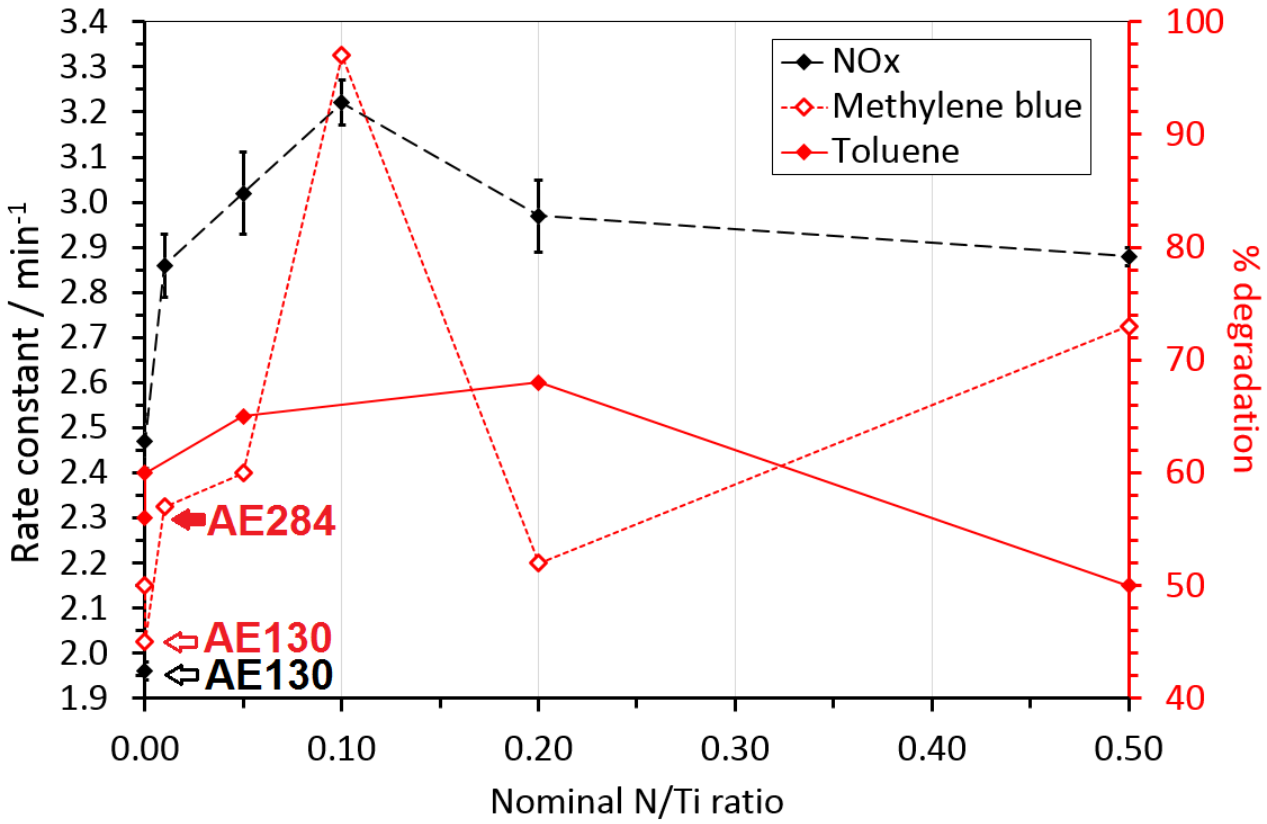

REFERENCES

[1] Spadavecchia, S., Cappelletti, G., Ardizzone S., Bianchi, C. L., Cappelli, S., Oliva, C., Scardi, P., Leoni, M., Fermo, P. Solar photoactivity of nano-N-TiO2 from tertiary amine: role of defects and paramagnetic species. *Appl. Catal. B: Environm*., **96**, 314–322 (2010).

[2] Larson, A.C., Von Dreele, R.B. *GSAS: General Structural Analysis System*, Los Alamos National Laboratory, Los Alamos, NM (1994)

[3]Ardizzone, S., Cappelletti, G., Fermo, P., Oliva, C., Scavini, M., Scimè, F. Structural and Spectroscopic Investigations of Blue, Vanadium-Doped ZrSiO4 Pigments Prepared by a Sol−Gel Route. *J. Phys. Chem. B*, **109**, 22112–22119 (2005).

[4] Kresse, G., Joubert, D. From ultrasoft pseudopotentials to the projector augmented-wave method. *Phys. Rev. B*, **59**, 1758–1775 (1999).

[5] Perdew, J. P., Wang, Y. Accurate and simple analytic representation of the electron-gas correlation energy. *Phys. Rev. B*, **45**, 13244–13249 (1992).

[6] Perdew, J. P., Burke, K. & Ernzerhof, M. Generalized Gradient Approximation Made Simple. *Phys. Rev. Lett*, **77**, 3865–3868 (1996).

[7] Dudarev, S., Botton, G., Savrasov, S., Humphreys, C., Sutton, A. Electron-energy-loss spectra and the structural stability of nickel oxide: An LSDA+U study. *Phys. Rev. B*, **57**, 1505–1509 (1998).

[8] Di Liberto, G., Pifferi, V., Lo Presti, L., Ceotto, M., Falciola, L. Atomistic Explanation for Interlayer Charge Transfer in Metal–Semiconductor Nanocomposites: The Case of Silver and Anatase. *J. Phys. Chem. Letters*, **8**, 5372–5377 (2017).

[9] Cheng, H., Selloni, A. Energetics and diffusion of intrinsic surface and subsurface defects on anatase TiO2(101). *J. Chem. Phys*., **131**, 054703 (2009).

[10] C. Marchiori, G. Di Liberto, G. Soliveri, L. Loconte, L. Lo Presti, D. Meroni, M. Ceotto, C. Oliva, S. Cappelli, G. Cappelletti, C. Aieta, S. Ardizzone, Unraveling the Cooperative Mechanism of Visible-Light Absorption in Bulk N,Nb Codoped TiO2 Powders of Nanomaterials. *J. Phys. Chem. C*, **118**, 24152–24164 (2014).

[11] L. Rimoldi, C. Ambrosi, G. Di Liberto, L. Lo Presti, M. Ceotto, C. Oliva, D. Meroni, S. Cappelli, G. Cappelletti, G. Soliveri, and S. Ardizzone, Impregnation versus Bulk Synthesis: How the Synthetic Route Affects the Photocatalytic Efficiency of Nb/Ta:N Codoped TiO2 Nanomaterials. *J. Phys. Chem. C*, **119**, 24104–24115 (2015).

[12] Meroni, D., Lo Presti, L., Di Liberto, G., Ceotto, M., Acres, R. G., Prince, K. C., Bellani, R., Soliveri, G., Ardizzone, S. A Close Look at the Structure of the TiO2‑APTES Interface in Hybrid

Nanomaterials and Its Degradation Pathway: An Experimental and Theoretical Study. *J. Phys. Chem. C*, **121**, 430–440 (2016).

[13] Tersoff, J. Theory of semiconductor heterojunctions: The role of quantum dipoles. *Phys. Rev. B*, **30**, 4874–4877 (1984).

[14] Tersoff, J. Schottky barriers and semiconductor band structures. *Phys. Rev. B*, **32**, 6968–6971 (1985).

[15] Cardona, M., Christensen, N. E. Acoustic deformation potentials and heterostructure band offsets in semiconductors. *Phys. Rev. B*, **35**, 6182–6194 (1987).

[16] Schleife, A., Fuchs, F., Rödl, C., Furthmüller, J., Bechstedt, F. Branch-point energies and band discontinuities of III-nitrides and III-/II-oxides from quasiparticle band-structure calculations. *Appl. Phys. Lett*., **94**, 012104 (2009).

[17] R. Dovesi, R. Orlando, A. Erba, C. M. Zicovich-Wilson, B. Civalleri, S. Casassa, L. Maschio, M. Ferrabone, M. De La Pierre, P. D'Arco, Y. Noel, M. Causa, M. Rerat, B. Kirtman. CRYSTAL14: A program for the ab initio investigation of crystalline solids. *Int. J. Quantum Chem.* **114**, 1287 (2014).

[18] R. Dovesi, V. R. Saunders, C. Roetti, R. Orlando, C. M. Zicovich-Wilson, F. Pascale, B. Civalleri, K. Doll, N. M. Harrison, I. J. Bush, P. D'Arco, M. Llunell, M. Causà and Y. Noël. *CRYSTAL14 User's Manual*, University of Torino, Torino, Italy (2014).

[19] Adamo, C., Barone, V. Toward reliable density functional methods without adjustable parameters: The PBE0 model. *J. Chem. Phys*., **110**, 6158–6170 (1999).

[20] Bader, R. F. A quantum theory of molecular structure and its applications. *Chem. Rev.*, **91**, 893–928 (1991).

[21] Tang, W., Sanville, E., Henkelman, G. A grid-based Bader analysis algorithm without lattice bias. *J. Phys.: Cond. Matter*, **21**, 084204 (2009).

[22] Van de Walle, C. G.; Martin, R. M. ''Absolute'' deformation potentials: Formulation and ab initio calculations for semiconductors. *Phys. Rev. B* **1987**, *35*, 8154.

[23] D'Amico, N. R.; Cantele, G.; Ninno, D. First principles calculations of the band offset at $SrTiO_3$−TiO_2 interfaces. *Appl. Phys. Lett.* **2012**, *101*, 141606.

[24] Di Liberto, G., Tosoni, S., Pacchioni, G. Role of Heterojunction in Charge Carrier Separation in Coexposed Anatase (001)-(101) Surfaces *J. Phys. Chem. Lett.* **2019**, *10*, 2372.

[25] Weston, L., Tailor, H., Krishnaswamy, K., Bjaalie, L., Van de Walle, C. G. Accurate and efficient band-offset calculations from density functional theory*Comput. Mater. Sci.* **2018**, *151*, 174.

[26] Ju, M.-G., Sun, G., Wang, J., Meng, Q., Liang, W. Origin of High Photocatalytic Properties in the Mixed-Phase TiO2: A First-Principles Theoretical Study. *ACS Appl. Mater. Interfaces* **2014**, *6*, 12885.

[27] Buckeridge, J., Butler, K. T., Catlow, C. R. A., Logsdail, A. J., Scanlon, D. O., Shevlin, S. A., Woodley, S. M., Sokol, A. A., Walsh, A. Polymorph Engineering of TiO2: Demonstrating How Absolute Reference Potentials Are Determined by Local Coordination. *Chem. Mater.* **2015**, *27*, 3844.

[28] Di Paola, A., Bellardita, M., Palmisano, L. Brookite, the Least Known TiO_2 Photocatalyst. *Catalysts* **2013**, *3*, 36.

[29] Spadavecchia, F.,Cappelletti, G., Ardizzone, S. Bianchi, C., Cappelli. S., Oliva, C., Scardi, P., Leoni, M., Fermo, P. Solar photoactivity of nano-N-TiO_2 from tertiary amine: role of defects and paramagnetic species. *Appl. Catal. B: Environmental* **96**, 314-322 (2010).